Deep-Sea Research, Vol. 36, No. 6, pp. 935–956, 1989.
Printed in Great Britain.

0198-0149/89 $3.00 + 0.00

A tracer study of the deep Gulf Stream cyclonic recirculation

ROBERT S. PICKART*† and NELSON G. HOGG*

(*Received* 21 *March* 1988; *in revised form* 23 *January* 1989; *accepted* 26 *January* 1989)

Abstract—An advective–diffusive numerical model is used to interpret water sample data from beneath the thermocline in the region of the Gulf Stream and deep western boundary current (DWBC), west of the Grand Banks. The nearly homogenized distributions of salinity and oxygen suggest that substantial cyclonic recirculation of the deep Gulf Stream comes in close contact with DWBC, which is the source of the tracers. The exchange of properties between the two flows is studied in order to relate tracer distributions to particular characteristics of the Gulf Stream gyre. Using a corresponding diffusion box model, it is shown that spin-up and the onset of homogenization in the gyre is controlled by diffusion from the boundary, and that the level of tracer in the gyre can be insensitive to the strength of lateral diffusivity (the salt case), but is strongly sensitive to vertical mixing (the oxygen case). The presence of vertical mixing, however, does not inhibit the occurrence of homogenization. The lateral (κ) and vertical (ν) diffusivities of the Gulf Stream gyre can be deduced by applying the model results to the observed oxygen distribution, and this leads to estimates of $\kappa \sim 10^6$ cm^2 s^{-1}, $\nu \sim 10$ cm^2 s^{-1}. The tight lateral extent of the recirculation, as suggested by the model results, agrees well with existing current meter data from the region.

1. INTRODUCTION

THE long characteristic time scales and small strength of the ocean's abyssal general circulation has made description and understanding of it slow and painstaking. As a result, the structure of the time-averaged flow in many areas is not well known. Despite the fact that the Gulf Stream system is one of the most thoroughly studied oceanic phenomena, its deep flow is only partially explored.

One of the well-known observational descriptions of the deep Gulf Stream was by WORTHINGTON (1976), who proposed the existence of a single anticyclonic gyre recirculating roughly 60 Sv of water. Since WORTHINGTON's (1976) work, two very different abyssal flow patterns have been proposed by WUNSCH and GRANT (1982) and HOGG (1983), also based on observations. The prominent feature in both of these studies is the presence of substantial cyclonic recirculation.

The collection of long-term deep current meter measurements in the region of the Gulf Stream has grown considerably in recent years, and was used by HOGG (1983) and HOGG *et al.* (1986) (hereafter referred to as H86) to show that a deep cyclonic gyre appears to be situated between the New England seamounts and Grand Banks (Fig. 1), transporting about 20 Sv. Such a recirculation, which is substantially smaller in lateral extent than the cyclonic flow proposed by WUNSCH and GRANT (1982), is strikingly similar to HOGG and

* Woods Hole Oceanographic Institution, Woods Hole, MA 02543, U.S.A.
† Present address: Graduate School of Oceanography, University of Rhode Island, Narragansett, RI 02882, U.S.A.

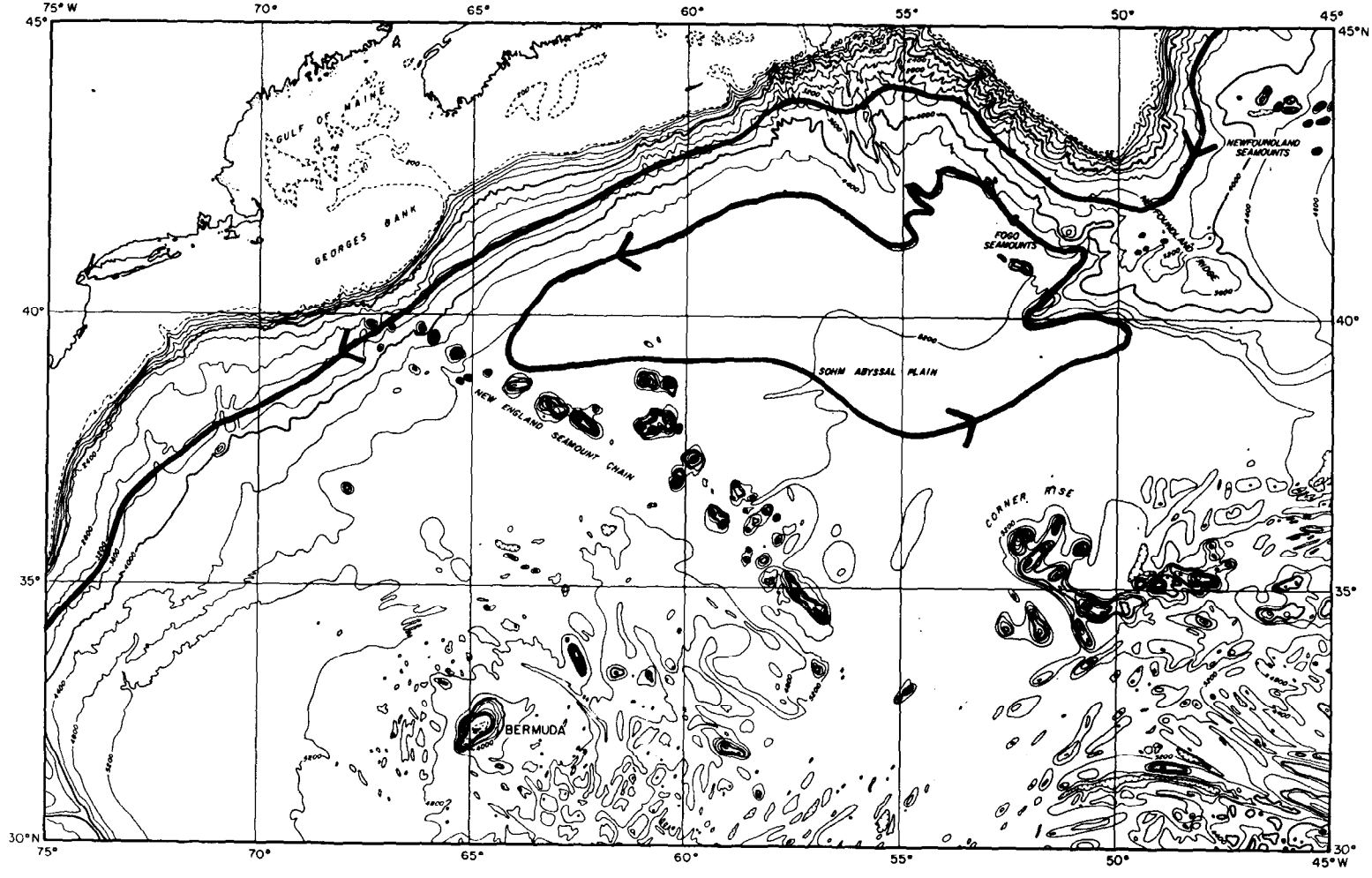

Fig. 1. A streamline of the deep Gulf Stream recirculation gyre and deep western boundary current, from PICKART (1988). The boundary current streamline is deduced from tracer measurements and the gyre streamline is from HOGG and STOMMEL's (1985) dynamical model of the cyclonic recirculation.

STOMMEL's (1985) prediction of cyclonic recirculation based on the assumption of uniform potential vorticity in the region. In addition to this evidence, RICHARDSON (1985) constructed an average velocity section along 55°W using a combination of surface drifter, SOFAR float and current meter data which show nearly barotropic recirculation to the north and south of the Gulf Stream. H86 mapped various tracers on density surfaces in this region which revealed the homogenization of properties, also suggestive of recirculating flow.

Tracers are particularly useful to study in this region because the cyclonic Gulf Stream gyre, which H86 termed the northern recirculation gyre (NRG), comes in close contact with the deep western boundary current (DWBC) west of the Grand Banks (Fig. 1). The DWBC is made up of relatively young water and has distinct signals in oxygen, silica and other properties that diffuse into the interior and hence are a source of tracers for the recirculation. In this work we analyse an advective–diffusive numerical model of the DWBC–NRG system, and apply the results to the observed deep tracer distributions. The model, which is described partly in H86, consists of a simplified gyre alongside a deep boundary current, implemented in order to study the manner in which the NRG influences tracer spreading laterally from the DWBC. Certain aspects of the model spin-up are discussed in PICKART (1988). In addition to the numerical model, a simple box model of the regional tracer budget is presented which aids considerably in the interpretation of the numerical results.

Two different tracers are considered in detail: salinity and oxygen. As noted by H86, their lateral distributions along a deep isopycnal in the NRG differ slightly, perhaps due to cross-isopycnal mixing. In Sections 2–4 we present the formulation and analysis of the numerical model and corresponding box model. Vertical mixing can be included parametrically in each of these models, and the cases with and without vertical mixing are considered separately and contrasted. In Section 5 some of the model results are applied to the tracer data set used by H86. Using the two models several conclusions can be made concerning the characteristics of the NRG.

2. NUMERICAL MODEL DESCRIPTION

We assume that the transfer of tracers from the DWBC to the NRG occurs along density surfaces, subject also to cross-isopycnal mixing. Consider the vertical profiles of oxygen and salinity (Fig. 2) from a CTD station occupied in the NRG (typical of the entire region). At the density of the DWBC core (average depth ~ 3600 m) the salinity distribution decreases monotonically with depth, but the oxygen profile has a relative maximum at this level. Thus, there is an upward and downward flux of oxygen out of the deep layer, whereas salt is fluxed into the layer from above and out of the layer into the bottom water. This implies that the net effect of cross-isopycnal mixing in the deep layer is more pronounced for oxygen than for salinity, and we assume therefore that the vertical mixing of salt is negligible. If in addition there is no cross-isopycnal flow, then this suggests that even though salinity is an active tracer we should in this context be able to model it as passive, since along isopycnals the only mechanism for salinity to change density is through cross-isopycnal transfer.

The three-dimensional advective–diffusive governing equation is

$$\frac{\partial \theta}{\partial t} + \mathbf{u} \cdot \nabla_h \theta + w \frac{\partial \theta}{\partial z} = \kappa \nabla \cdot \nabla_h \theta + \nu \frac{\partial^2}{\partial z^2} \theta, \tag{1}$$

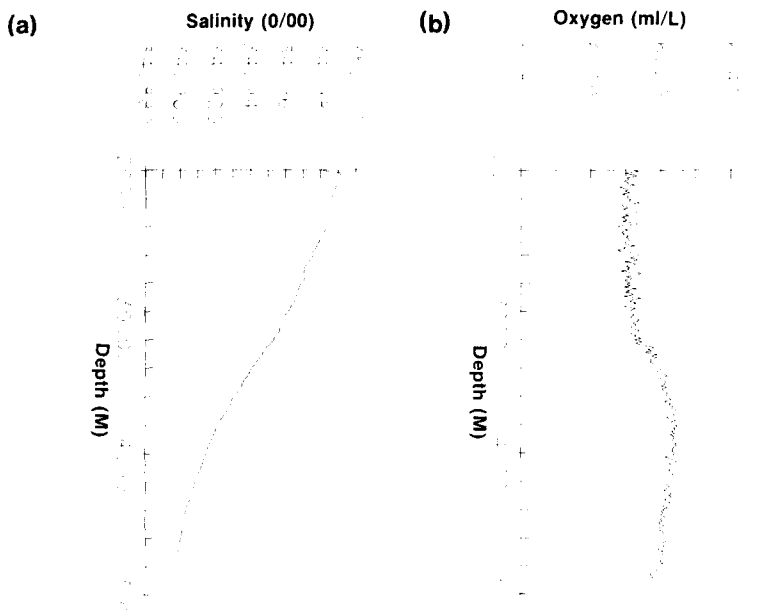

Fig. 2. (a) CTD profile of salinity vs depth below 2000 m for OC134 Sta. 40 in the NRG. (b) Oxygen profile.

where $\theta(x, y, z, t)$ is the tracer concentration, $\mathbf{u}(x,y,z)$ is the horizontal velocity vector, $w(x,y,z)$ is the vertical velocity, $\nabla_h = \mathbf{i}\partial/\partial x + \mathbf{j}\partial/\partial y$, and κ, ν are the lateral, vertical eddy diffusivity (assumed constant). We are interested in the evolution of tracer in the deep layer which we assume is bounded above and below by density surfaces that are nearly flat so that x and y are considered to be along-isopycnal and z cross-isopycnal.

The deep horizontal velocity vector can be expressed in terms of the geostrophic steamfunction (assuming constant Coriolis parameter) $\mathbf{u} = \mathbf{k} \times \nabla_h \psi$. The vertical velocity can be obtained from the density equation (assumed steady), which is a balance between vertical (cross-isopycnal) advection and vertical diffusion of potential density ρ,

$$w\rho_z = \nu\rho_{zz}.$$

We assume in the model that the vertical diffusion of density in the deep layer is negligible (i.e. the right-hand side of the above equation is identically zero), and correspondingly $w = 0$. For an equation of state of the form

$$\rho = \rho_0(1 - \alpha(T - T_0) + \beta(S - S_0)),$$

where T is the potential temperature, and S is the salinity, if we assume that a T–S relation exists for the deep layer then no vertical diffusion of density implies that $T_{zz} = S_{zz} \pm 0$, i.e. the potential temperature and salinity decrease linearly with depth. Note that this is consistent with the cross-isopycnal flux of salinity described above.

In a finite-difference sense we represent the vertical tracer structure with three grid points, the center grid point corresponding to the concentration in the center of the deep layer. The upper and lower grid points are fixed boundary conditions representing

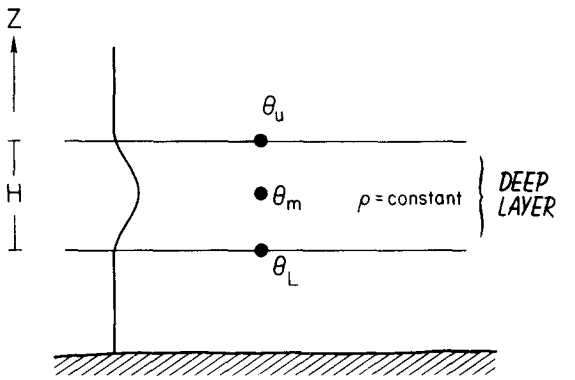

Fig. 3. Vertical resolution of the deep layer in the numerical model. Three grid points are used to represent a continuous profile like that shown.

reservoir values above and below the deep layer (Fig. 3). Applying this approximation to (1) (with $w = 0$) gives,

$$\frac{\partial \theta_M}{\partial t} + u\frac{\partial \theta_M}{\partial x} + v\frac{\partial \theta_M}{\partial y} = \kappa\left(\frac{\partial^2 \theta_M}{\partial x^2} + \frac{\partial^2 \theta_M}{\partial y^2}\right) - \frac{8\nu}{H^2}\left(\theta_M - \frac{\theta_U + \theta_L}{2}\right),$$

where θ_M is the value of tracer at the center of the layer, θ_U, θ_L are the values of upper, lower reservoir (these are assumed constant), and H is the layer thickness. In terms of the anomaly $\theta' = (\theta_M - (\theta_U + \theta_L)/2)$ this equation becomes

$$\frac{\partial \theta'}{\partial t} + u\frac{\partial \theta'}{\partial x} + v\frac{\partial \theta'}{\partial y} = \kappa\left(\frac{\partial^2 \theta'}{\partial x^2} + \frac{\partial^2 \theta'}{\partial y^2}\right) - \frac{8\nu}{H^2}\theta'. \tag{2}$$

Equation (2) is quasi-three-dimensional in that it contains a parameterization of the vertical mixing; note that this vertical flux term has the form of Newtonian damping. H86 showed that for the length scales involved here this type of oxygen depletion in the abyssal layer overwhelms any biological consumption that may be occurring. In modelling the salinity it is assumed that $(\theta_U + \theta_L)/2 \approx \theta_M$ (i.e. $\theta' \approx 0$, Fig. 3) so that the vertical flux is not large enough to affect the distribution. For oxygen it is assumed that $(\theta_U + \theta_L)/2 < \theta_M$ and the flux term is retained.

The model circulation is shown in Fig. 4, to be compared with the streamlines of Fig. 1. A Gaussian source of tracer is maintained across the upstream (northern) edge of the boundary current; tracer fills the current and then diffuses into the interior, eventually becoming entrained within the gyre. PICKART (1988) has previously analysed one aspect of the salinity simulation, the occurrence of homogenization in the gyre. Here we look at the broader perspective of the boundary current as a tracer source to the gyre, taking into account the various sinks of tracer as well.

3. THE MODEL WITH NO VERTICAL DIFFUSION

We consider first equation (2) (dropping the primes) without the vertical flux term. To obtain solutions the equation is finite-differenced in the horizontal (approximately 10,000

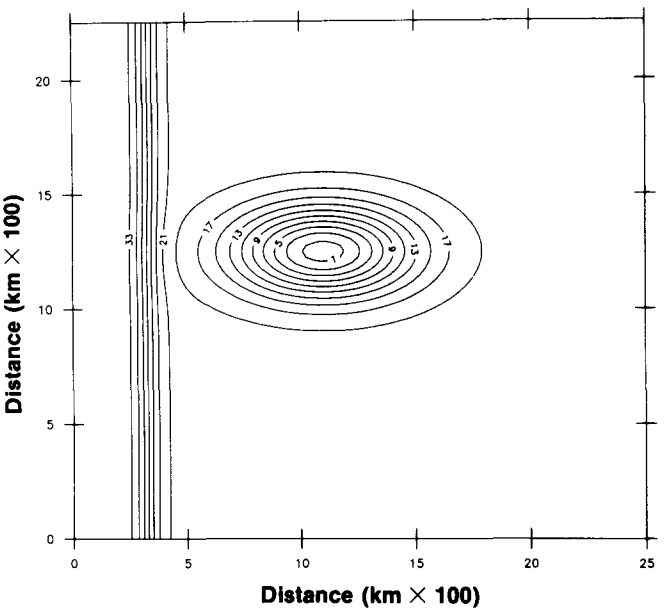

Fig. 4. Streamlines of the numerical model boundary current and gyre, from PICKART (1988). Contour values are in Sverdrups (assuming a vertical extent of 1000 m).

grid points) and numerically integrated. The advection is calculated using upstream differencing and the diffusion by centered differencing. Implicit diffusion is kept to a minimum by use of a reverse-diffusion time step (SMOLARKIEWICZ, 1983). Other than along the upstream edge of the boundary current where tracer is input, tracer exits the domain by two mechanisms: advection by the boundary current and diffusion along the entire boundary. The latter process occurs by use of an open boundary condition which quantitatively simulates the diffusive mechanism [PICKART (1988) gives a detailed description of the open boundary condition]. Steady state is ultimately reached when there is a balance between the various cross-boundary fluxes. Two different lateral diffusivities were considered, $\kappa \sim 10^6 \text{cm}^2\ \text{s}^{-1}$ and $\kappa \sim 5 \times 10^6 \text{cm}^2\ \text{s}^{-1}$; the corresponding numerical simulations are hereafter referred to as κ_1 and κ_5.

At the start of each simulation the domain is tracer-free. As tracer first advects downstream in the boundary current and spreads laterally, its eastward flux into the interior is inhibited by the westward flow of the gyre and accentuated by the gyre's eastward flow. The plume of tracer that emanates from the boundary is displaced somewhat to the south of the region of maximum eastward flow of the gyre, rather than coincident with the core of the flow. Once within the gyre the tracer plume spirals across gyre streamlines towards the center, and tracer begins accumulating there [see PICKART (1988) for details of the gyre entrainment].

Throughout the simulation the gradient of tracer across the gyre remains fairly weak, and at steady state complete homogenization occurs. Figure 5 shows the accumulation of tracer at the center of the gyre vs time (this is the last place in the domain to reach steady state). All the numerical simulations were halted when the yearly accumulation rate in the gyre center fell below 2% of the earlier maximum rate. It is shown that when

this happens the gyre has attained a level of tracer greater than 95% of its asymptotic value, and so this is taken to be steady state. There are two interesting points to be made about Fig. 5. First, it took over three times longer for steady state to be reached in the smaller diffusivity simulation (an e-folding time of ~80 years vs ~25 years). Second, the value of the homogenized plateau is approximately the same at steady state for both cases.

RHINES and YOUNG (1983) showed that the time scale for homogenization to occur within a gyre is the diffusive time of the gyre. We wish to compare this to the e-folding times observed in Fig. 5. Since the spin-up times of the two simulations differ by only a factor of 3, it is not sufficient to consider merely order of magnitude estimates; we must use the precise expression for the diffusive time of an elliptical gyre. PICKART (1987) showed that the appropriate time scale is

$$\tau_G = \frac{L_Z L_M}{\kappa}\left(.42\,\frac{L_x L_y}{L_x^2 + L_y^2}\right). \tag{3}$$

where L_x and L_y are the x and y length scales of the gyre, and L_Z and L_M are the zonal and meriodional scales of homogenization. The term inside the parentheses represents the deviation from a simple order of magnitude scale analysis estimate.

The scales L_Z and L_M take on different values for the two simulations being considered, as the homogenized region is smaller for larger κ. In κ_1 homogenization occurs to the $\psi = 16$ streamline, while in κ_5 it occurs only to the $\psi = 9$ streamline (Fig. 6). Substituting the appropriate values into (3) gives a diffusive time of 5 years for κ_1 and 0.5 years for κ_5. Comparing these values to the actual times we see that in the first simulation spin-up is 15 times longer than the diffusive time of the gyre, and in the second it is 50 times longer.

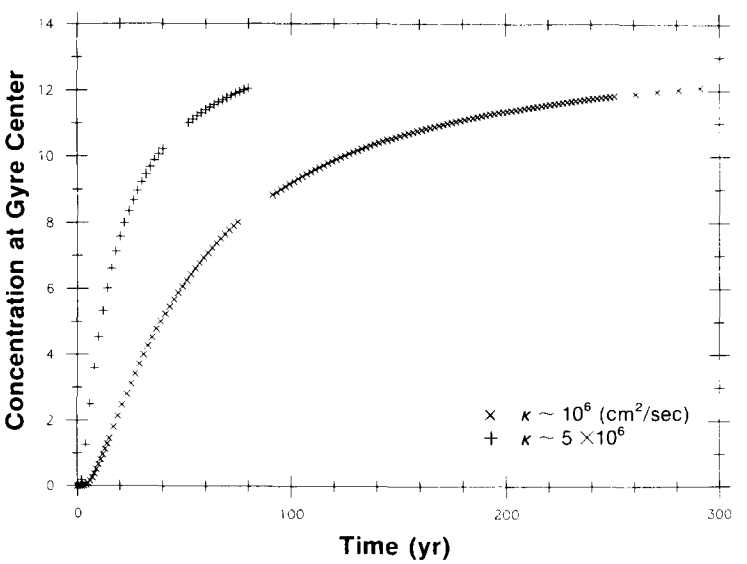

Fig. 5. Time history of tracer accumulating at the center of the gyre for two different diffusivities.

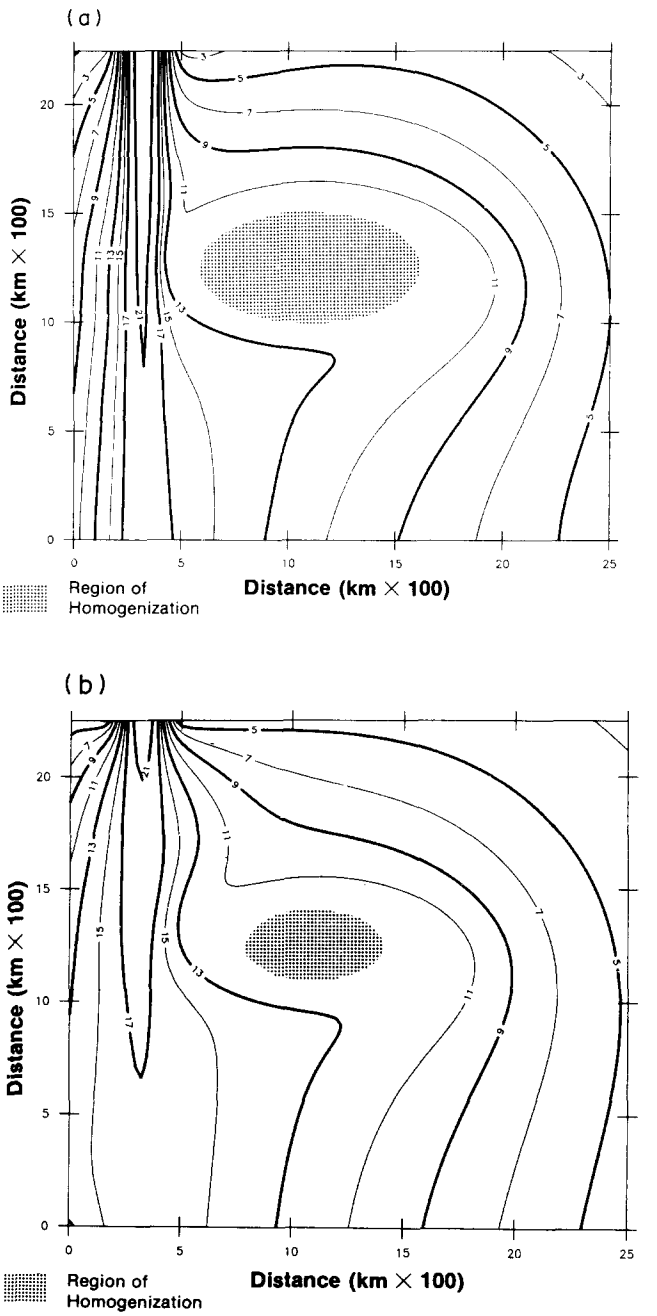

Fig. 6. Distribution of tracer at steady state (the salt case) for (a) $\kappa \sim 10^6$ cm^2 s^{-1} and (b) $\kappa \sim 5 \times 10^6$ cm^2 s^{-1}, from PICKART (1988). The Gaussian source has a peak value = 25.

In light of the character of the spin-up this result is not surprising. It is evident since the tracer level throughout the gyre rises uniformly that the rate of spin-up is being controlled by the diffusion of tracer from the boundary current (i.e. it takes very little time for tracer to diffuse throughout the gyre once it reaches the gyre's edge). In order to quantify this idea, as well as understand what factors dictate the final level of the homogenized plateau in the gyre, a simple box model is examined below.

3.1. *Diffusive box model*

In the strongly advective limit of the numerical model (under which condition homogenization occurs) it is the slow diffusive processes that regulate the spin-up and dictate the net transfer of properties into the interior. It is instructive then to consider the domain of the numerical model as being composed of several subregions which only communicate with one another diffusively. Along with this we also consider a simplified spin-up process by assuming that the plume of tracer which penetrates the gyre gets pulled precisely around a streamline (i.e no spiral occurs, consistent with the notion of strong advection).

The four subregions of the domain that we consider are depicted in Fig. 7. The first region corresponds to the boundary current. Advection from the northern source fills this region quickly and continually acts to maintain its level of tracer. The second is the outer edge of the gyre. Tracer diffuses into this region from the boundary current and then "instantaneously" gets pulled around the circuit. From here the tracer diffuses inward to the center of the gyre (the third region) and outward to the vast surrounding area (the fourth region).

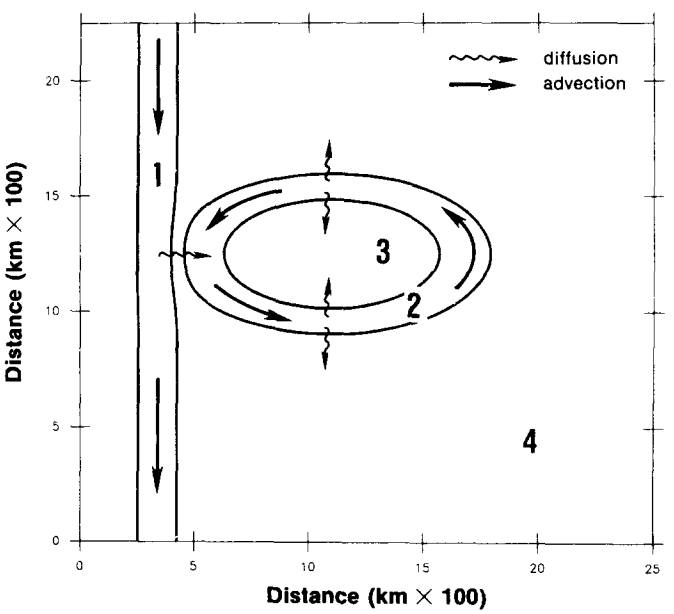

Fig. 7. Domain of the diffusive box model consisting of four subregions; tracer is transferred into adjacent regions by diffusion only. The time scale of diffusion from region 1 to 2 is τ_B, from 2 to 3 is τ_G, and from 2 to 4 is τ_R.

Each subregion of the domain is represented by a single concentration, and the transfer of tracer between regions is characterized by a set of diffusive time scales, with the strength of the flux proportional to the difference in concentrations. Because of the strong advective input into the boundary current region the concentration here is fixed throughout the spin-up. Also, we take the fourth region to be an infinitely large background reservoir whose value cannot be altered and so is set equal to zero. This means that there are only two active regions in the box model, those comprising the gyre. The governing equations for the gyre edge and gyre center are

$$\frac{d\phi_e}{dt} = \frac{(\Phi - \phi_e)}{\tau_B} + \frac{(\phi_c - \phi_e)}{\tau_G} + \frac{(0 - \phi_e)}{\tau_R}$$
$$\frac{d\phi_c}{dt} = \frac{(\phi_e - \phi_c)}{\tau_G}, \tag{4}$$

where ϕ_e is the concentration of gyre edge, ϕ_c is the concentration of gyre center, Φ is the concentration of boundary current (fixed), τ_B is the boundary time scale (diffusion between boundary current and gyre edge), τ_G is the gyre time scale (diffusion between gyre edge and gyre center), τ_R is the reservoir time scale (diffusion between gyre edge and background reservoir). The initial conditions are $\phi_c = \phi_e = 0$ at $t = 0$.

It is convenient to express solutions to (4) in terms of the non-dimensional parameters representing the relative sizes of the three diffusive time scales,

$$\Delta_{GB} = \frac{\tau_G}{\tau_B}, \Delta_{GR} = \frac{\tau_G}{\tau_R}, \Delta_{BR} = \frac{\tau_B}{\tau_R} = \frac{\Delta_{GR}}{\Delta_{GB}}.$$

It is not obvious *a priori* what the magnitudes of these parameters are. However, the results of the numerical model can be used to constrain them.

The solutions ϕ_e and ϕ_c are of the form

$$\phi(t) = \phi_0 + \phi_1 e^{-t/\tau_1} + \phi_2 e^{-t/\tau_2}, \tag{5}$$

where ϕ_0 is the steady-state value, and the other terms are transients. Of the transients the slower mode (taken here to be τ_2) dictates the spin-up of the system, and so the spin-up time is defined as $\tau = \tau_2$ and can be expressed as

$$\tau = S(\Delta_{GB}, \Delta_{GR})\tau_G, \tag{6}$$

where the function S is defined as

$$S(\Delta_{GB}, \Delta_{GR}) = \frac{2}{2 + (\Delta_{GB} + \Delta_{GR}) - [(\Delta_{GB} + \Delta_{GR})^2 + 4]^{1/2}}.$$

The value of S represents the length of spin-up relative to the diffusive time of the gyre. Recall that the time scale for homogenization to occur in the numerical model is much greater than the diffusive time of the gyre ($\tau \gg \tau_G$), which means that $S \gg 1$. This in turn implies that both Δ_{GB} and Δ_{GR} are $\ll 1$. We can determine the relative magnitude of these two parameters by examining the level of tracer in the gyre. In expression (5) the steady-state value for the gyre center can be expressed as

$$\phi_0 = P(\Delta_{BR})\Phi, \tag{7}$$

where the function P is defined as

$$P(\Delta_{BR}) = \frac{1}{1 + \Delta_{BR}}.$$

The value of P represents the fraction of tracer relative to the boundary current input value which accumulates in the gyre (note that P depends only on Δ_{BR} which measures the relative size of Δ_{GB} and Δ_{GR}). We saw above that the concentration of the homogenized region in the numerical model gyre is independent of diffusivity, which suggests that in the box model the parameter Δ_{BR} should take on the same value in each case. To determine this value we can match (7) to the level of the homogenized plateau. To do this, however, we need to equate the boundary current input value Φ to an appropriate quantity in the numerical model. In the box model Φ does not depend on diffusivity (it is a boundary condition); since the total amount of tracer in the numerical model boundary current does vary with the size of κ (compare Fig. 6a and b), we use the peak concentration of the upstream boundary condition as the value for Φ. This is justified in that the box model is based on the presumption of strong advection, and in the extreme advective limit the entire numerical boundary current will equilibrate to the input Gaussian distribution, in which case the peak concentration is the appropriate choice.

The steady-state concentration of the gyre is approximately one half the peak concentration of the upstream input (Fig. 6), which implies that $\Delta_{BR} \sim 1$, or that the time scale for equilibration of the gyre edge to the boundary input value is also the time scale of decay of the gyre edge into the background reservoir. The reason why these two processes occur at roughly the same rate is that whereas diffusion from the boundary is much stronger, diffusion into the background reservoir occurs over a much greater area and these effects cancel one another.

So by matching the expressions (6) and (7) to the numerical model solutions, we obtain the following ordering of the diffusive time scales:

$$\tau_G \ll \tau_B \sim \tau_R. \tag{8}$$

The box model now can be simplified by setting Δ_{BR} identically equal to one ($\tau_B = \tau_R$), which means solutions are now expressible in terms of a single non-dimensional parameter

$$\Delta = \frac{\tau_G}{\tau_B} \ll 1. \tag{9}$$

Expressions (6) and (7) simplify to

$$\tau = S(\Delta)\tau_G, \tag{10}$$

where

$$S(\Delta) = \frac{1}{1 + \Delta - (\Delta^2 + 1)^{\frac{1}{2}}} \approx \frac{1}{\Delta},$$

and

$$\phi_0 = \frac{\Phi}{2}. \tag{11}$$

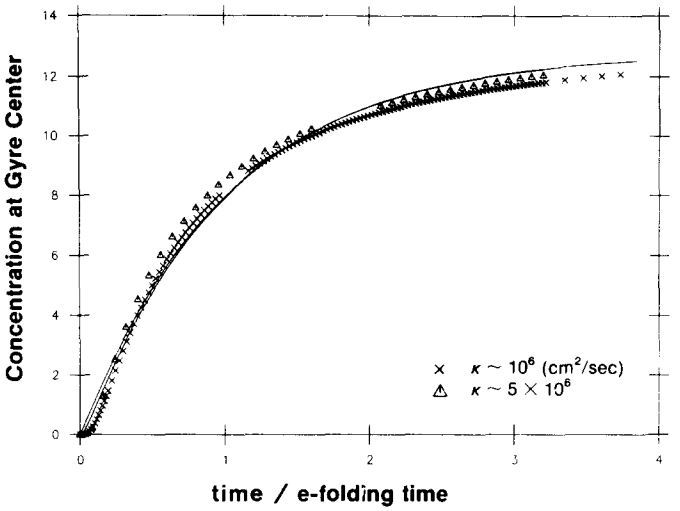

Fig. 8. The accumulation curves of Fig. 5, only the time axis has been normalized for each curve by the associated spin-up time. The solid lines are the box model predictions for the gyre center.

The parameter Δ measures the relative strengths of the two fundamental time scales of the system. We can now explain quantitatively how diffusion from the boundary controls the spin-up. When $\Delta \to 0$, $\tau \to \tau_B$ and the system spins-up on the boundary time scale (i.e. once tracer diffuses from the boundary to the edge of the gyre it then quickly spreads into the gyre center). This is the case in the numerical model. In the opposite limit of $\Delta \to \infty$, $\tau \to \tau_G$, which corresponds to the RHINES and YOUNG (1983) case in which spin-up occurs on the gyre time scale. In this case the edge of the gyre equilibrates quickly and tracer then slowly diffuses into the center. By matching (10) to the numerical solutions using the gyre diffusive times estimated above for the κ_1 and κ_5 simulations, we determine the corresponding values of Δ (referred to as Δ_1 and Δ_5). Then we can use the box model to predict the level of tracer at the center of the numerical model gyre as a function of time.

Recall that both ϕ_c and ϕ_e consist of a steady term and two transient modes (expression 5). It is the case that for small Δ the faster transient decays so quickly that it can be neglected. Normalizing the time axis of Fig. 5 by the appropriate spin-up times then allows the κ_1 and κ_5 simulations to be compared in Fig. 8, which also contains the corresponding ϕ_c solutions from the box model normalized in a similar fashion. It is seen that the two simulations collapse to a single case and agree reasonably well with the box model predictions. Note that both the κ_1 and κ_5 curves extend to beyond three e-folding times, which means that in each case the gyre has reached >95% of its asymptotic level of approximately $\Phi/2(=12.5)$. The associated ϕ_e curves (not shown) closely resemble those for the gyre center, consistent with the numerical result that the level of tracer throughout the gyre rises at nearly the same rate.

4. THE MODEL WITH VERTICAL DIFFUSION

We now consider the presence of vertical mixing (the oxygen case) which is incorporated into the numerical model as the damping term in (2). We take $\theta_U = \theta_L = 0$ (Fig. 3)

so that the vertical anomaly is just equal to the concentration in the center of the deep layer. Two different simulations were done, the first with $\nu = 1$ cm^2 s^{-1}, $H = 1000$ m and the second with $\nu = 2$ cm^2 s^{-1}, $H = 750$ m (roughly three times stronger vertical mixing). These simulations are referred to as ν_1 and ν_2, respectively (in both cases $\kappa \sim 10^6$ cm^2 s^{-1}).

During spin-up tracer diffuses from the boundary current to the gyre in much the same manner as in the previous simulations with only lateral diffusion. However, a marked difference between the salt and oxygen cases occurs at steady state. The steady-state distribution of ν_2 appears in Fig. 9, to be compared with Fig. 6a (κ_1), which has the same lateral diffusivity but no vertical flux. Note that concentrations in the boundary current are similar in the two simulations; however, the level of tracer in the gyre is substantially smaller in ν_2. This is because the strong flow of the boundary current does not allow fluid to spend enough time in this region to be significantly influenced by vertical mixing; it is only while tracer diffuses slowly from the boundary current into the interior that vertical mixing becomes prominent and acts as a sink, substantially reducing the spin-up time of the system as well. The small amount of tracer that does penetrate the gyre does so similarly to κ_1; however, the slight bowl-shaped tracer distribution across the gyre remains a permanent feature in the steady state of ν_2 rather than giving way to complete homogenization as in κ_1.

At steady state there can be no net flux of tracer into the region bounded by a streamline of the gyre. In κ_1 this is accomplished at the center of the gyre by way of homogenization. In the oxygen case the vertical flux out of the gyre center must be balanced by an inward lateral flux across streamlines (hence the bowl-shaped distribution). Integrating the steady form of (2) within a gyre streamline and applying the

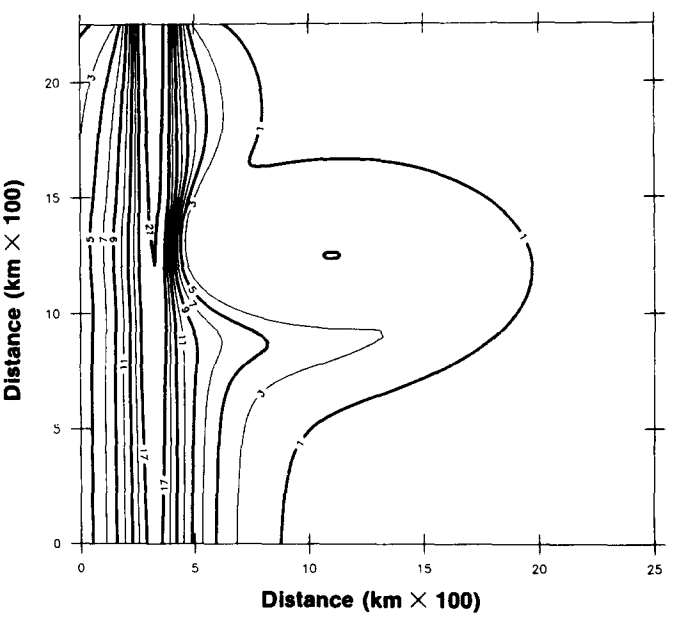

Fig. 9. Steady-state distribution of tracer (the oxygen case) for $\kappa \sim 10^6$ cm^2 s^{-1}, with the addition of vertical mixing in which $\nu \sim 2$ cm^2 s^{-1}. The same Gaussian source is applied as in the salt case.

divergence theorem gives,

$$\frac{8\nu}{H^2}\int\int_A \theta dA = \kappa \oint_S \frac{\partial\theta}{\partial n}\, dS, \tag{12}$$

where A is the area enclosed within the streamline S, and n is normal to the streamline. This results in the following relationship between ν and κ,

$$\nu = \left(\frac{\oint_S \partial\theta/\partial n\, dS}{8\nu/H^2 \int\int_A \theta\, dA}\right)\kappa. \tag{13}$$

We applied expression (13) to the steady-state distribution of ν_2 and were able to recover the value of ν knowing κ (2.3 cm^2 s^{-1} vs the actual value of 2.0 cm^2 s^{-1}).

4.1. *Box model with vertical mixing*

The diffusive box model developed above can be modified to include the effects of vertical diffusion as well. The layers directly above and below the deep layer (represented by θ_L and θ_U in the numerical model) can be thought of as together forming another subregion of the box model domain which is in contact with the gyre only. It is not in contact with the boundary current because tracer flushes through this region too quickly to be altered by vertical diffusion, and it is not in contact with the background reservoir for the trivial reason that this reservoir is void of tracer. Because the new region represents a vast area as well, it to is taken to be a reservoir whose value cannot be changed and is thus set equal to zero.

Even though we are including another region in the box model it is not an active one, and a third governing equation is not required. There is however another time scale,

$$\tau_V = \frac{H^2}{8\nu},$$

which is the diffusive time for tracer to decay into the vertical reservoir. The appropriate set of equations is,

$$\begin{aligned}\frac{d\phi_e}{dt} &= \frac{(\Phi-\phi_e)}{\tau_B} + \frac{(\phi_c-\phi_e)}{\tau_G} + \frac{(0-\phi_e)}{\tau_B} + \frac{(0-\phi_e)}{\tau_V},\\ \frac{d\phi_c}{dt} &= \frac{(\phi_e-\phi_c)}{\tau_G} + \frac{(0-\phi_c)}{\tau_V}.\end{aligned} \tag{14}$$

Note that we have set $\tau_R = \tau_B$ as before because the relation (8) must still apply. The initial conditions are the same as before: no tracer in the gyre. When $\tau_V \to \infty$ (i.e. no vertical reservoir) the set (14) collapses to (4).

As before, it is convenient to express the solutions to (14) in terms of non-dimensional parameters. With the addition of τ_V we introduce another parameter,

$$\varepsilon = \tau_G/\tau_V, \tag{15}$$

in addition to $\Delta(= \tau_G/\tau_B)$ defined previously. Since both the numerical simulations with vertical mixing, ν_1 and ν_2, have $\kappa \sim 10^6$ cm^2 s^{-1} (the value in κ_1) we set $\Delta = \Delta_1$, this way

isolating the effect of vertical mixing within the context of the numerical results previously presented. Solutions of (14) are thus expressed in terms of the single parameter ε, measuring the relative strength of lateral vs vertical diffusion.

Because the expanded box model does not require a third governing equation, the solutions for ϕ_c and ϕ_e are still of the form (5). The spin-up time is defined as before (the time scale of the slower mode), which is now expressed as

$$\tau = S_1(\varepsilon)\tau_0(\Delta_1), \tag{16}$$

where

$$S_1(\varepsilon) = \frac{1}{1 + \varepsilon/(1 + \Delta_1 - (\Delta_1^2 + 1)^{\frac{1}{2}})},$$

and $\tau_0(\Delta_1)$ is spin-up time of the system with no vertical diffusion [i.e. expression (10) evaluated at $\Delta = \Delta_1$]. We saw earlier that $\tau_0(\Delta_1) \approx \tau_B$, so the function S_1 simply measures spin-up relative to the boundary diffusive time. In the limit $\varepsilon \to \infty$ (strong vertical diffusion), spin-up occurs on the other fundamental time scale ($\tau \to \tau_V$). The graph of S_1 vs ε appears in Fig. 10.

In addition to the spin-up time, the other major difference with the inclusion of vertical mixing is the reduced level of tracer in the gyre at steady state. Recall that without vertical diffusion the final gyre level is independent of Δ (expression 11), or, in terms of the numerical model, independent of the lateral diffusivity. When vertical

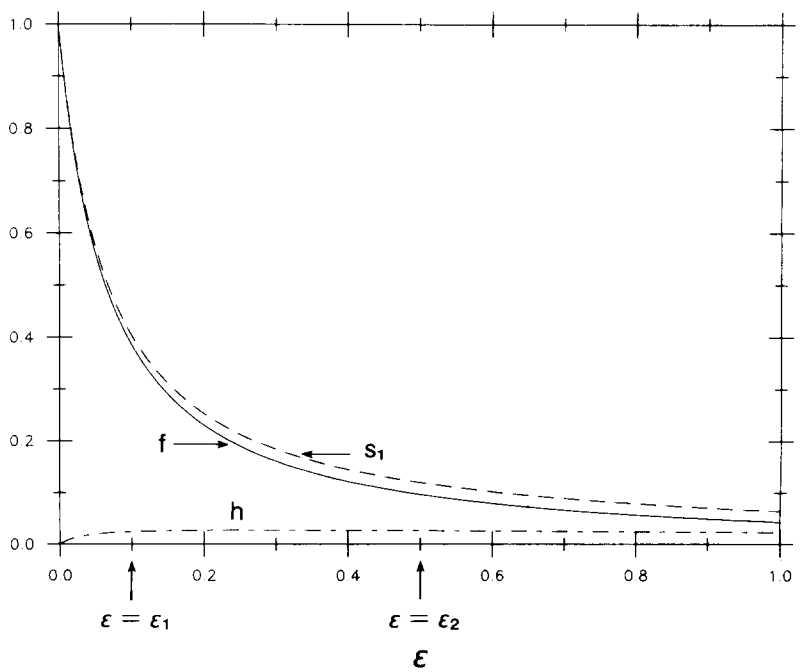

Fig. 10. Amplitude of the box model spin-up time (S_1), final gyre level (f), and homogenization (h) as affected by the presence of vertical mixing. The strength of the mixing is measured by the parameter ε; the values of ε associated with simulation v_1 and v_2 are indicated by ε_1 and ε_2, respectively.

diffusion is added not only is the gyre level dependent on the strength of the vertical diffusion, it becomes dependent on the strength of the lateral diffusion as well. At steady state the expression for the gyre level is

$$\phi_0 \sim f(\varepsilon)\frac{\Phi}{2}, \tag{17}$$

where

$$f(\varepsilon) = \frac{\Delta_1}{\Delta_1 + \Delta_1\varepsilon + \varepsilon^2/2}.$$

The function f plotted vs ε (Fig. 10) measures the fraction of tracer in the gyre relative to the level when there is no vertical diffusion.

Recall that, without vertical mixing, the evolution of ϕ_c is nearly identical to that of ϕ_e, and that in the large time limit $\phi_c \to \phi_e$ (i.e. complete homogenization occurs). With the addition of vertical mixing, it is not surprising that this no longer is the case. In the steady-state distribution of ν_2 (Fig. 9) the concentration of tracer within the gyre is characterized by a slight minimum at the gyre center. The equivalent to this in the box model is the fact that $\phi_c(t \to \infty) < \phi_e(t \to \infty)$. The significance of this feature is measured by the function h,

$$h(\varepsilon) = \frac{\phi_c(t \to \infty) - \phi_e(t \to \infty)}{\Phi - \phi_e(t \to \infty)} = \frac{\Delta_1\varepsilon}{\Delta_1 + \Delta_1\varepsilon + 2\varepsilon + \varepsilon^2},$$

which compares the gradient of tracer off the boundary to the gradient across the gyre. The plot of h vs ε also appears in Fig. 10.

It is interesting to note in Fig. 10 that whereas the spin-up time and final level of tracer in the gyre are extremely sensitive to vertical mixing, the degree of homogenization (as measured by h) remains virtually the same, i.e. the gyre is always homogenized. For very strong mixing the vertical reservoir draws away most of the tracer, so homogenization occurs in the sense that the gyre is uniformly void of tracer. Using the previously computed values of τ_G and the appropriate values of ν and H, the parameter ε can be calculated for the ν_1 and ν_2 simulations. It is found that ν_1 corresponds to moderate vertical mixing and ν_2 to strong vertical mixing (the values of ε so computed, ε_1 and ε_2, are marked in Fig. 10). As before, the box model solutions for the gyre center agree nicely with the numerical results.

5. COMPARISON TO DATA

In this section we apply various results of the preceeding model study to salinity and oxygen measurements from this region of the North Atlantic. The data comes from six recent hydrographic surveys, most of it from a single cruise OC134 in the summer of 1983. The salinity has an uncertainty of ±0.002‰ and the oxygen ±0.04 ml l^{-1}. Because all the measurements were calibrated using bottle data, however, the expected errors should be even less, especially for oxygen; this is attested to by the mapability of the signals over a number of different cruises. A detailed description of the data set and accompanying error analysis appears in H86.

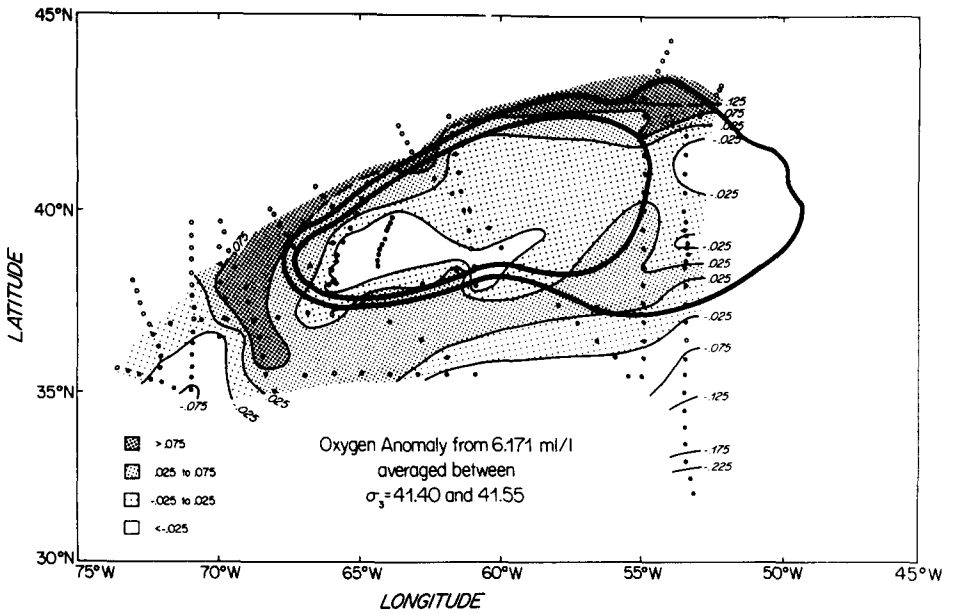

Fig. 11. Lateral map of oxygen anomaly in the deep layer (from H86).

5.1. *Homogenization*

The lateral oxygen distribution in the deep layer from H86 (Fig. 11) is characterized by strong gradients off the continental boundary that merge into a broad region which is nearly uniform (further to the south the level once again drops off). A plume of high oxygen emanates from the boundary near 68°W and extends well into the interior. From this distribution and a similar one for salinity, H86 computed a corresponding average section across the gyre through the boundary current (Fig. 12), showing that both tracers exhibit homogenization in the region of the NRG although the oxygen distribution has a slight minimum within this region (centered at 41°W) suggestive of vertical mixing.

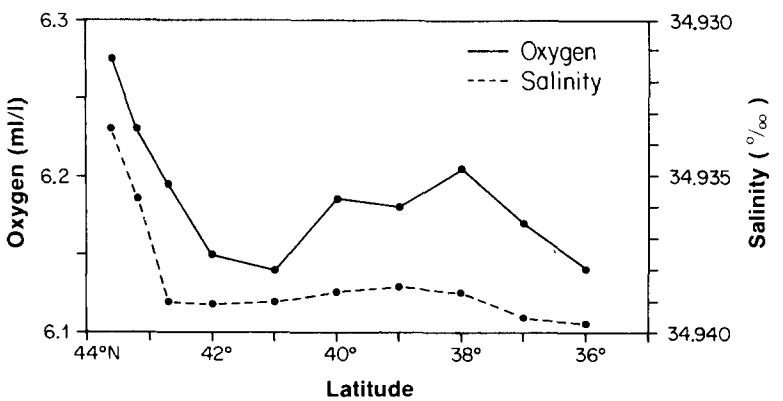

Fig. 12. Average sections of oxygen and salinity through the DWBC and NRG (from H86). The graph plots the average concentration of successive lateral strips parallel to the DWBC vs the latitude of the strip at 55°W.

Superimposed on the contour map of oxygen are two "streamlines." The outer one was constructed using a closed deep layer isopach in this region (from HOGG and STOMMEL, 1985) as a guide. The inner one was then subjectively constructed to fit within the region spanned by the tracer measurements (using the outer streamline as a guide). Note that the high oxygen plume leaves the boundary downstream of where the outer streamline turns offshore, consistent with the numerical model results and further supporting the claim by H86 for tight recirculation. This ridge of high oxygen then proceeds to penetrate the gyre in a manner similar to the model. Although the ridge is very slight this does not imply that the vertical mixing is weak, as was shown in the above box model.

5.2. *Oxygen flux balance*

We saw above that the integrated balance (12) for the area enclosed by a gyre streamline gives a relationship between the lateral and vertical diffusivities (13). This can be applied to the NRG oxygen distribution of Fig. 11 within the area of the inner streamline. In (13) recall that the value of θ is actually the vertical anomaly, $\theta = \theta_M - (\theta_U + \theta_L)/2$ (Fig. 3). In the model we set $\theta_U = \theta_L = 0$, but in the ocean this is certainly not true and to apply (13) we must determine an estimate of the upper and lower layer reservoir values.

Consider again the oxygen profile in Fig. 2 for a station in the center of the NRG. The profile is asymmetric in that the value above the deep signal is smaller than that below it. (This is true of nearly all of the stations in the data set.) Consequently, the oxygen flux through the top of the deep layer is greater than that through the bottom, and in fact this downward flux can be neglected. With this simplification, the value of the vertical mixing parameter in (2) decreases by a factor of two and the oxygen anomaly simplifies to $\theta = \theta_M - \theta_U$ [expression (13) is altered accordingly]. We choose the layer thickness to be $H = 2500$ m, and for each station equate θ_M with the deep relative maximum in the oxygen profile and θ_U with the value 1250 m above this (θ_M so defined conforms roughly to an isopycnal surface). Using this definition of the anomaly, the denominator in (13) was estimated for the region within the inner streamline of Fig. 11. To compute the value of the line integral in (13) we break the streamline into two parts, a northern half and a southern half, and use a single value of $\partial\theta/\partial n$ for each piece calculated from the average section in Fig. 12. Finally, the expression inside the parentheses in (13) is estimated, which gives the following relationship between the diffusivities,

$$\nu \approx (10^{-5})\kappa. \tag{18}$$

5.3. *Oxygen level*

We now address the question of how much oxygen is contained within the NRG with regard to the DWBC source. Using the diffusive box model we obtained a functional relationship (17) between the concentration of the gyre center and boundary input. This expression depends on the various time scales τ_B, τ_G and τ_V, but also relies implicity on the fact that the lateral and vertical background reservoirs are tracer-free. As this is not true in the ocean, we must alter (17) in order to apply it to the data.

We define ϑ as the value of both background reservoirs as well as the initial concentrations of ϕ_c and ϕ_e. When this is incorporated into the set of equations (14), the

result (17) for the steady-state concentration of tracer at the gyre center becomes,

$$\phi_o \sim f(\varepsilon)\frac{\Phi}{2} + \left(1 - \frac{f(\varepsilon)}{2}\right)\vartheta, \tag{19}$$

where the second term on the right-hand side represents the correction due to the non-zero background ϑ.

In the data we can readily measure the equivalent of ϕ_0, the concentration at the center of the gyre. However, in order to apply (19) we must identify the boundary conditions Φ and ϑ. Consider first the boundary input value Φ. We saw in Section 3.1 that in terms of the numerical boundary current the appropriate input value is the concentration at the core of the current. In light of Fig. 1 we choose the DWBC core concentration at 50°W as the input value for (19) (upstream from here tracer diffusing from the DWBC "misses" the NRG). It is not straightforward to identify the background reservoir value ϑ in the data, and we treat it as the unknown in (19). This quantity is similar to the diffusivity in that we are unable to measure it directly, but can say whether or not an estimate is plausible. For a comparison we use the average concentration in the upper layer, $\overline{\theta_U}$ (defined in Section 5.2).

To solve (19) for ϑ we need to know the value of f, which depends on the parameters Δ and ε [defined by (9) and (15)]. Estimating the area of oxygen homogenization from Fig. 11 we can calculate the values of ε and Δ for a range of possible diffusivities constrained by (18). It turns out, however, that for realistic values of κ and ν the predicted values of ϑ from (19) are significantly larger than $\overline{\theta_U}$; in other words the box model predicts a smaller concentration of oxygen than that observed in the NRG. This discrepancy is reconciled below by considering a variation in the numerical model streamfunction.

5.4. *Western intensification*

Admittedly there is some question as to the validity of using $\overline{\theta_U}$ as a measure of the "background" oxygen concentration surrounding the deep layer. This being the case, an inconsistency regarding the oxygen level in the NRG should not in itself be cause to restructure the numerical model or box model. In addition there is uncertainty in the flux balance (18), and it is possible that this does not express the true relationship between the lateral and vertical diffusivities. Nonetheless it is desirable to fit all the pieces of the calculation together in a consistent fashion and offer the result as one interpretation of the data.

The velocity field of the numerical model was chosen as a simplified representation of the DWBC/NRG system. It is, however, certainly not the only streamfunction that could have been used, although it is hoped that employing a similar flow field would not alter major results of the model. Because of the inconsistency above we now consider a variation in the streamfunction which influences the flux of tracer into the gyre. The current meter data that Hogg (1983) used to describe the NRG are somewhat sparse, allowing for some leeway in specifying a corresponding simulated flow field.

There are several ways that the gyre velocity field can be altered to cause tracer to accumulate at a faster rate. We choose here to consider the effect of western intensification, in which the southward flow of the gyre is made comparable in strength to the

boundary current (which remains unaltered). A single experiment, abbreviated ω_1, was done in which $\kappa \sim 10^6$ cm s^{-1} (lateral diffusion only, same value as in κ_1). As a result of the increased speed with which tracer is transported into the interior, the center of the gyre is filled at a faster rate than in κ_1. This does not mean, however, that more tracer ultimately diffuses into the gyre, and in fact the gyre level again asymptotes to the same value as in κ_1 (and κ_5), which means only that the spin-up time is shorter. Since more tracer is needed in the gyre to reconcile the above discrepancy, it might seem that altering the streamfunction in this way is not useful. However, when vertical diffusion is added the spin-up time is reduced even more, and this in turn permanently preserves any differences in the transient states of ω_1 and κ_1, in particular the fact that early on there is more tracer in the western intensified gyre.

In order to apply this result to the oxygen data we must re-compute the values of the box model parameters Δ and ε for a western intensified NRG. Recall that $\Delta = \tau_G/\tau_B$ and $\varepsilon = \tau_G/\tau_V$. We need the numerical model to compute τ_B, the spin-up time of the system ($\tau \sim \tau_B$); the other two times scales τ_G and τ_V are computed directly from the data. Note then that the time scale τ_B is the only one of the three time scales that is different in the western intensified case, so only the value of Δ will be changed from before (made somewhat larger), in turn increasing the value of f in (19).

As shown in Fig. 13 we are now able to get reasonably good agreement between the measured oxygen background concentration $\overline{\theta_U}$ and a predicted value of ϑ (solid circle), corresponding to the diffusivity pair of $\kappa \sim 10^6$ cm^2 s^{-1} and $\nu \sim 10$ cm s^{-1}. Note that the accompanying value of f is approximately 0.4, which says that the level of oxygen in the NRG is roughly 40% of what it would be if there were no vertical mixing. Also shown in the figure are the resulting predictions if we ignore the flux balance constraint (18) and arbitrarily set $\nu = 1$. In that case the vertical flux is extremely weak which results in comparatively small background concentrations.

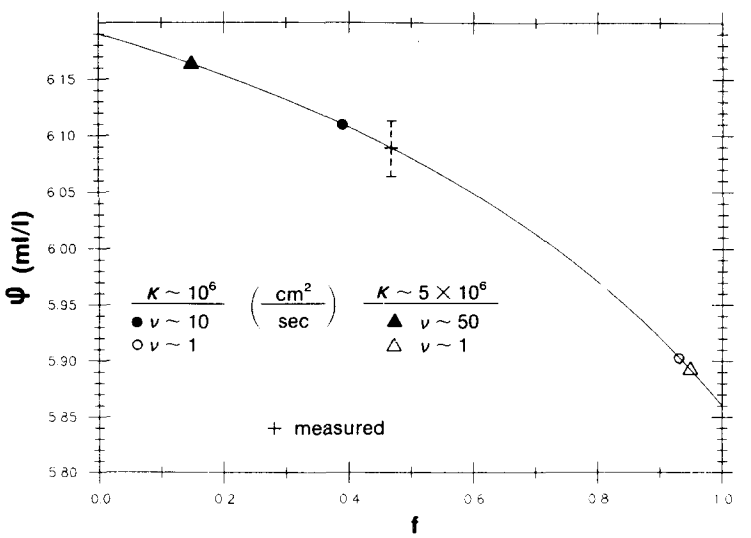

Fig. 13. Oxygen background concentration ϑ predicted using the box model. The values for the examples discussed in the text are shown in comparison to the measured quantity $\overline{\theta_U}$ (cross).

A value of 10 $cm^2\ s^{-1}$ for ν is substantially larger than various estimates of the vertical diffusivity at thermocline depths (for instance ROOTH and OSTLUND, 1972). However, values as large as 3–4 $cm^2\ s^{-1}$ have been calculated for Antarctic bottom water flowing northward along the western boundary of the South Atlantic (HOGG *et al.*, 1982; WHITEHEAD and WORTHINGTON, 1982). The value of $\kappa \sim 10^6\ cm^2\ s^{-1}$ on the other hand is smaller than many estimates found in the literature. For example, direct estimates of κ were made using SOFAR float data from the MODE region (28°N, 69°W) by FREELAND *et al.* (1975), who calculated a value of $7 \times 10^6\ cm^2\ s^{-1}$. Using the same technique J. PRICE (personal communication) computed values in the range of $1.5 - 8.2 \times 10^7\ cm^2\ s^{-1}$ for the LDE region (31°N, 70°W). It should be noted, however, that these estimates are for the thermocline, and Price detects a decrease in the size of κ with depth.

6. CONCLUSION

Two types of tracers have been studied using a simple numerical model representing the cyclonic recirculation of the deep Gulf Stream alongside the DWBC. The first type (salinity) is governed by lateral processes only, whereas the second type (oxygen) is influenced by vertical mixing as well. Interestingly, when vertical mixing is absent the final level of tracer in the gyre seems to be independent of the strength of the lateral mixing (provided it is weak).

A box model simplification of the numerical model showed explicitly how the gyre level is dictated by the core concentration of the boundary current and the values of lateral and vertical diffusivity. When the vertical mixing is identically zero the dependence of the gyre level on lateral diffusion drops out as well, provided the nondimensional parameter $\Delta_{BR} = \tau_B/\tau_R$ remains constant (which is the case in the numerical model). Homogenization within the gyre is a rigorous feature of the system and occurs regardless of the strength of the vertical diffusion. Spin-up of the system is slower than might be suggested by the size of the homogenized region because it is dictated by the slow diffusion of tracer from the boundary current (modified by diffusion vertically out of the domain).

In addition to illuminating some of the numerical model results, the box model was used to apply these results to the data. In the deep layer there is a broad region of homogenized properties to the south of the DWBC (centered at roughly 60°W) suggestive of closed circulation. The plume of oxygen extending from the DWBC into the interior delimits the southern extent of the gyre and serves as additional evidence for tight recirculation. In contrast to salinity, the distribution of oxygen has a slight minimum in the center of the gyre due to vertical mixing. The resulting fluxes of oxygen imply oceanic mixing coefficients of $\kappa \sim 10^6\ cm^2\ s^{-1}$ and $\nu \sim 10\ cm^2\ s^{-1}$, which allow the NRG to accumulate only 40% of the oxygen that is available from the DWBC.

Acknowledgements—We wish to thank Dale Haidvogel for help in developing the numerical model and interpreting the results. Bill Young gave us useful ideas and suggestions regarding the model study. This work was supported by the Office of Naval Research through contracts N00014-76-C-0197 and N00014-84-C-0132, NR 083-400; and N00014-82-C-0019 and N00014-85-C-0001, NR 083-004, and the National Science Foundation through grant OCE82-14925. Contribution No. 6715 from the Woods Hole Oceanographic Institution.

REFERENCES

FREELAND H. J., P. B. RHINES and T. ROSSBY (1975) Statistical observations of the trajectories of neutrally buoyant floats in the North Atlantic. *Journal of Marine Research*, **33**, 383–404.

HOGG N. G. (1983) A note on the deep circulation of the western North Atlantic: its nature and causes. *Deep-Sea Research*, **30**, 945–961.

HOGG N. G. and H. STOMMEL (1985) On the relationship between the deep circulation and the Gulf Stream. *Deep-Sea Research*, **32**, 1181–1193.

HOGG N. G., P. BISCAYE, W. GARDNER and W. J. SCHMITZ Jr (1982) On the transport and modification of Antarctic Bottom Water in the Vema Channel. *Journal of Marine Research*, Supp. **40**, 231–263.

HOGG N. G., R. S. PICKART, R. M. HENDRY and W. J. SMETHIE Jr (1986) The northern recirculation gyre of the Gulf Stream. *Deep-Sea Research*, **33**, 1139–1165.

PICKART R. S. (1987) The entrainment and homogenization of tracers within the cyclonic Gulf Stream recirculation gyre. Ph.D. Thesis, Massachusetts Institute of Technology and Woods Hole Oceanographic Institution, Woods Hole, MA.

PICKART R. S. (1988) Entrainment and homogenization of a passive tracer in numerical model gyre. *Journal of Geophysical Research*, **93**, 6761–6773.

RHINES P. B. and W. R. YOUNG (1983) How rapidly is a passive scaler mixed within closed streamlines? *Journal of Fluid Mechanics*, **133**, 133–145.

RICHARDSON P. L. (1985) Average velocity and transport of the Gulf Stream near 55W. *Journal of Marine Research*, **43**, 83–111.

ROOTH C. G. and H. G. OSTLUND (1972) Penetration of tritium into the Atlantic thermocline. *Deep-Sea Research*, **19**, 481–492.

SMOLARKIEWICZ P. K. (1983) A simple positive definite advection scheme with small implicit diffusion. *Monthly Weather Review*, **111**, 479–486.

WHITEHEAD J. A. Jr and L. V. WORTHINGTON (1982) The flux and mixing rates of Antarctic Bottom Water within the North Atlantic. *Journal of Geophysical Research*, **87**, 7903–7924.

WORTHINGTON L. V. (1976) On the North Atlantic circulation. *The Johns Hopkins Oceanographic Studies*, **6**, 110pp.

WUNSCH C. and B. GRANT (1982) Towards the general circulation of the North Atlantic Ocean. *Progress in Oceanography*, **11**, 1–59.